Master of Science Thesis:

Diffusion Tensor Imaging in the Cervical Spinal Cord

Implementing methods for acquisition, processing and evaluation

---

Filip Szczepankiewicz

Supervisors:

Jimmy Lätt
Markus Nilsson
Johanna Mårtensson

Department of Medical Radiation Physics, Clinical Sciences, Lund
Lund University, Sweden
Submitted August 2011
Revised September 2011

Abstract

Diffusion tensor magnetic resonance imaging (DT-MRI or DTI) is an imaging technique that is sensitive to the diffusion movement of water contained in tissue. It is used to quantify parameters such as the diffusivity and its directionality. Because diffusion is intimately connected to the tissue microarchitecture DTI is one of the few techniques that can quantify tissue microstructure non-invasively *in vivo*. Further, it has been established that DTI parameters such as mean diffusivity and fractional anisotropy are sensitive to the influence of a variety of diseases, among them are neurodegenerative diseases such as multiple sclerosis. Although still in its cradle several papers have reported successful implementation of DTI in the spinal cord, noting that there are still challenges to be solved before it can be clinically implemented.

The aim of this work was to create, optimize and implement a DTI protocol of the cervical spine in a clinical setting and to evaluate its potential as a complement to current conventional diagnostics.

The main work was performed using the Siemens Skyra (3T) located at the Lund University Hospital. The imaging protocol was based on similar protocols used in DTI of the brain although several modifications were implemented to adapt the acquisition to the anatomically complicated region of the spine. The protocol was designed to include three imaging series; the main DTI series; a turbo spin echo (TSE) reference series for distortion correction purposes; and a high resolution T2-weighted series for conventional diagnostics. An automated tractography based segmentation method was devised to facilitate fast and reproducible evaluation of the DTI parameters.

The method was tested by means of validation and an *in vivo* pilot study. Validation was performed to gauge system performance. The pilot study was performed as a proof of concept for the acquisition, processing and evaluation methods.

Results show that using DTI parameters for individual diagnostics is currently limited by the large inter and intra-subject variation, however the *in vivo* pilot study proved the suggested methods to be viable in a clinical setting; adding only 5 minutes to the standard scan time and allowing for quick and highly automated evaluation of data which is suitable for large group comparisons.

Abbreviations

AP	Anterior to posterior direction
ADC	Apparent diffusion coefficient
C1 to C7	Cervical vertebrae, denoted with number
CNS	Central nervous system
CSF	Cerebrospinal fluid
DFC	Dynamic field correction
DT	Diffusion tensor
DTI	Diffusion tensor imaging
DT-MRI	Diffusion tensor magnetic resonance imaging
DTT	Diffusion tensor tractography
EC	Eddy-current
EPI	Echo planar imaging
FA	Fractional anisotropy
FFS	Feet first supine
FOV	Field of view
GDC	Geometrical distortion correction
GM	Gray brain matter
HFS	Head first supine
IS	Inferior to superior direction
MD	Mean diffusivity
MR	Magnetic resonance
MRI	Magnetic resonance imaging
MS	Multiple sclerosis
QuTE	Quantitative tractography evaluation
RL	Right to left direction
ROI	Region of interest
SNR	Signal to noise ratio
TE	Echo time
TR	Repetition time
TSE	Turbo spin echo
WM	White brain matter

1 Introduction

Magnetic resonance imaging (MRI) is an advanced medical imaging modality that enables non-invasive study of the human body. It has vast potential to explore the morphology of any part of the body but can also perform functional analysis by sensitizing images to perfusion, flow, oxygenation, diffusion and more.

As MRI is expanding it is vital to explore the capacity of new techniques to complement or replace what is considered as conventional diagnostics. An imaging technique that has shown great potential in the diagnostics and visualization of the central nervous system (CNS) is diffusion tensor imaging (DTI).

It is a relatively young technique but has already generated vast quantities of novel information about the brain. Its introduction to regions outside the brain has been delayed due to practical and technical restrictions although advances in software and hardware performance have made it possible to start assessing its usability in the spine.

1.1 Background

Diffusion weighted magnetic resonance imaging (DWI) is a widely used imaging technique applied predominately in the brain for diagnostics of diseases such as acute stroke [1, 2]. It sensitizes the image signal to the diffusion movement of water in tissue, making it one of few techniques that can probe the microstructure of tissue non-invasively [1, 3, 4]. It was first discovered to have a viable clinical application when Moseley *et al.* showed that DWI was sensitive to ischemic injury in cat brain much earlier post occlusion compared to conventional imaging [5]. Since then several advances have made diffusion-based MRI a powerful tool in both research as well as in clinical applications.

Incorporating information about the diffusion directionality, or so called diffusion anisotropy, using the relatively simple diffusion tensor (DT) model, opened up even more opportunities to describe the microstructural attributes of tissue in a way that morphological imaging could not [6, 7]. DTI not only presented new parameters that were related to tissue quality but the introduction of the tensor allowed for the directionality information to be depicted as continuous lines in 3D-space, creating what is known as diffusion tensor tractography (DTT). This visualization technique offers a unique ability to non-invasively depict the architecture [2] and connectivity [8, 9] of neural tissue as well as serve as a powerful segmentation tool to assist in the selection of specific white brain matter (WM) structures [4, 6, 7, 10-12].

The most common use of DTI and DTT is in the brain. It is a suitable subject organ to work with due to the macroscopic scale and high anisotropy of WM as well as its relatively homogenous environment.

As the quantification of DTI parameters is rooted in the microstructural configuration of the observed tissue it is interesting to know the intricate mechanics of diffusion in WM. The relative contributions of tissue components to anisotropy is not completely resolved, however, it is an intuitively attractive idea to relate the anisotropy to the microscopic heterogeneity [13] caused by a combined effect of the well-organized

structure of myelin sheaths, axons and neurofibrils restricting water diffusion in a macroscopically ordered fashion [1, 14].

The last decade has also seen the introduction of DTI research in the human spinal cord. Quantitative diffusivity maps of the human cervical spine were reported as early as 1999 by Clark *et al.* [15]. In this paper it was reported that the diffusivity parallel to the spine was several times higher than in the perpendicular direction implying a strong diffusion anisotropy presumed to reflect the structural directionality of the spinal WM.

Since then there has been a positive outlook for DTI and DTT to be used for a large variety of research and clinical queries. Suggestions for applications in neural tissue span widely including characterization of microstructural changes due to spondylosis [16], Brown-Séquard syndrome [11], schizophrenia, dyslexia, trauma, stroke, ageing [6, 17], tumors, ischemic and inflammatory lesions [7] as well as multiple sclerosis (MS) [18, 19]. The use of DTI and DTT has also been reported to include the conus and cauda eqina [20] as well as more peripheral neural tissue such as the lumbar nerve roots [21].

In 2008 Ellingson *et al.* published a paper for the first time mapping the DTI metrics for the entire length of the spine to be used as a base-line in clinical comparisons [22]. This was done using a ROI approach delineating the GM and WM manually in axial slices spanning from the first cervical to the first lumbar vertebrae for thirteen healthy volunteers.

Resolving the spinal structure even further Smith *et al.* segmented the spine into ventral, dorsal and lateral parts using a combination of ROI definition and tractography based voxel selection [12]. Even though the authors recognized that the structural composition at these sites is different with respect to axon diameter and myelin density, they found no significant difference in the DTI metrics. However, it is remarkable that they demonstrated the ability to evaluate specific sub-structures of the spinal cord using tractography based segmentation.

In the same year, Onu *et al.* published a similar paper reporting a significant difference in ventral, dorsal and lateral locations of the spine using both ROI and tractography based segmentation [4].

Although conventional MRI is sensitive to MS lesions it lacks in pathological specificity and ability to detect diffuse damage [23, 24], thus it is beneficial to use the ability of DTI and DTT to complement conventional imaging to further quantify pathologies in the central nervous system (CNS) such as MS [18].

MS is a chronic autoimmune disease of the brain and spinal cord with a peak onset in the ages between 20 and 40. The effect of MS is degeneration of the myelin sheaths that are insulating the axons, so called demyelination [23], in most cases leading to severe clinical disability [25]. Although the lesion damage in the brain can have severe consequences the acute symptoms are more often caused by damage in the spinal cord [26], further, the spinal cord damage has been suggested to be more indicative of patient disability than that of the brain [19].

In 2005 Rovaris *et al.* [24] summarized the reported findings concerning the effect of MS on DTI metrics in the brain. In WM it was consistently reported to increase the diffusivity and lower the anisotropy in lesions visible in conventional imaging as well as in normal appearing tissue. Although it would be natural to assume the same effect in the spinal WM the literature conflicts with respect to the diffusivity but is consistent in reporting a lower diffusion anisotropy in MS inflicted tissue [18, 24, 27].

In a recent study Van Hecke *et al.* [18] examined the spine of MS patients with lesions that were visible on conventional T2-weighted images as well as patients with normal appearing spinal cords. They found a significant difference in diffusion anisotropy between the healthy control and both patient groups. When comparing the two patient groups there was no significant difference implying that microstructural change due to MS involvement can, in cases of patients with seemingly unaffected spinal cords, only be detected with DTI. Van Hecke *et al.* also caution interpreting this as there being no significant difference in the tissue damage in the two patient groups, stating that this could be an effect of the small number of subjects.

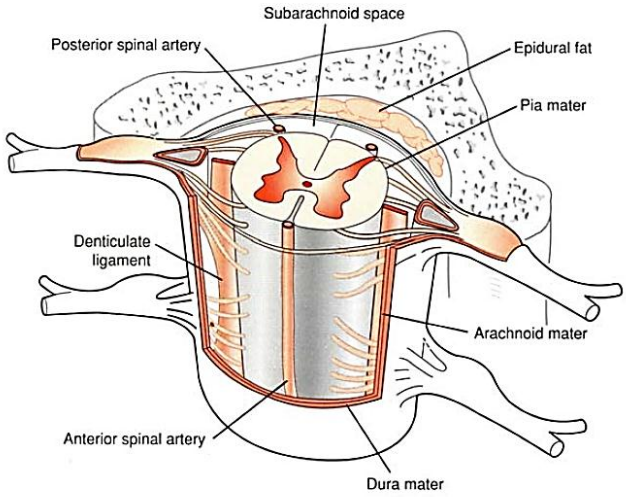

Figure 1 – Model of a spinal cord segment. The spine is enclosed in the spinal canal separated from the bony structures by several membranes and suspended in cerebrospinal fluid (CSF). In contrast to the brain the WM is on the outside and the GM is on the inside (butterfly shape). At the cervical level the spinal cord has a diameter of roughly 12 mm [6]. Looking at the spinal cord in detail it is evident that it is not constructed of homogenous WM but has a more complex structure. The figure exemplifies how a segment of the spinal cord contains perpendicularly extending nerves connecting the spine to peripheral parts of the body as well as the blood vessels in proximity to the spine. There are differences even within the WM. Different funiculi exhibit variation in cell architecture [12] and the shape as well as the relative amount of WM vs. GM changes over the length of the spine [22]. Image adapted from [28].

In light of these examples it is important to address the fact that DTI and DTT pose many challenges [3]. The disadvantages in the case of the spinal cord, compared to the brain, are mainly its relatively small size, its heterogeneous surroundings and the proximity to physiological movement.

The small size and complicated structure of the spinal cord, seen in Figure 1, combined with the typical DTI voxel size of 2.0×2.0×2.0 mm^3 gives rise to strong partial volume effect (PVE), biasing the measurement in voxels at tissue interfaces [4, 6, 17]. This can, to some extent, be avoided by using more restrained ROI definition methods or by using well-adjusted tractography for structure segmentation [6].

DTI of the spine suffers from significant image distortions. Due to the spinal cords proximity to tissue with heterogeneous susceptibility, such as the spinal column, lunges and esophagus, the local magnetic field is perturbed causing image distortions. There are also distortions due to eddy-currents (EC), subject motion, respiratory movement, swallowing movement, CSF pulsation and chemical shift [3, 6, 22]. EC can be minimized by using field correction techniques or post-hoc correction regimes that can also be used to correct for subject movement. Respiratory movement and CSF pulsation can be alleviated by respiratory and cardiac gating but these are usually not implemented.

Finally it should be recognized that there are precautions considering virtually every step of data acquisition, correction and evaluation. That is because parameter choice and evaluation methodology can have a significant influence on the end result [3, 29]. It is therefore advisable that in comparing any number of subjects the acquisition be kept exactly the same for each one and that the evaluation of data is made as objective as possible.

To this end DTT can be used as a powerful tool to segment the spine according to predefined thresholding parameters instead of using voxel selection through manual ROI delineation. This has been proven to decrease the user dependency [6] and could be used to facilitate faster segmentation for higher throughput [12].

1.2 Aim

The aim of this project was to evaluate the possibility to implement DTI of the cervical spine in a clinical setting, using a state-of-the-art 3T MRI scanner. To achieve this the project was divided into the following sub-objectives:

- To create an imaging protocol that could be used in clinical routines, with an acquisition time of 5 minutes or less
- To validate the system and the method through quality control
- To create and organize necessary tools for post-processing and evaluation of data
- To assess the potential of the method in a pilot study

2 Theory

2.1 Diffusion

Diffusion, also known as Brownian motion, is the general name for random particle translational movement, caused by internal kinetic energy, expressed in any given

medium. This transportation of matter can be observed in all materials, gas, liquid or solid. The diffusion in solid materials, compared to liquid and gas, is of course not as prominent since the inter-particle binding energy surpasses that of the kinetic energy working to break the lattice structure.

Diffusion is commonly divided into three types; free diffusion, hindered diffusion and restricted diffusion [30].

Free diffusion is present only when the diffusing particle encounters no impassable barriers or permeable obstructions during the observation time and is, with a few exceptions, isotropic because there is no influence present to impose a spatial dependency on the movement. The exception is found in some liquid crystals that express an anisotropic diffusion even in the absence of any mechanical influence [31, 32].

The diffusion of any medium is said to be hindered or restricted any time the diffusing particles interacts with anything other than the diffusing medium and can be both isotropic and anisotropic.

Hindered diffusion means that the particles are free to move any given length from their origin but must do so by passing some obstructions along the way, increasing the tortuosity of the medium [30].

Restricted diffusion entails a complete or partial confinement of the diffusing particle causing the apparent diffusivity to decrease as the range of diffusion exceeds the available volume [33-35]. Note that the diffusion might be both free or restricted depending on the time scale, *i.e.* the diffusion time, during which a given system is observed [33]. Consider, for example, a sphere with impenetrable walls filled with a liquid. Given enough time a particle that started at the very center of the sphere will have probed the entire volume of the sphere, no matter how big it is. In this case the particle cannot be said to be freely diffusing. If, on the other hand, the time during which we observed the particle was much shorter than the time required for it to sample all of the available space it would appear to be freely diffusing.

The diffusion directionality is determined by the structure of the tissue containing the diffusing particles [1]. If the random movement of the particles is asymmetrically restricted or hindered the diffusion is said to be anisotropic. This means that the diffusion of particles in the medium seems to have a preferred diffusion direction implying that their probability of translation is non-uniform with respect to direction in space.

Since restrictions on the diffusion occur in all kinds of tissue anisotropic diffusion at a microscopic level is always present to some degree but is mostly undetectable macroscopically due to the low conformity in the preferred direction [33]. Thus, for the anisotropy to be measurable in an MRI experiment the subject tissue needs to express directional conformity at a voxel scale. This large size and high conformity is present in the WM structures of the brain and spinal cord which makes them suitable for DTI and DTT.

2.2 Modeling isotropic diffusion

As an example of isotropic diffusion consider a drop of ink carefully suspended in water. If there is no bulk motion in the medium it is possible to see how the ink dot grows radially out from its origin and becomes more diluted. In this case the transport of ink particles out from the origin can be described by Fick's first law which states that there is a particle flux in the presence of a concentration inhomogeneity according to

$$\boldsymbol{J} = -D\nabla C \qquad \text{Eq. 1}$$

where $\boldsymbol{J}$ is the particle flux vector, D is the diffusion coefficient and ∇C is the particle concentration gradient [33]. The minus sign indicates that the net flow will be directed from regions of higher concentration to regions of lower concentration. The diffusion coefficient is determined by the temperature in the medium as well as the size and shape of the molecules that compose the medium [1, 31].

It can be shown that the probability density function P for a given translation $\boldsymbol{r} = (\boldsymbol{r_2} - \boldsymbol{r_1})$, from the particle origin $\boldsymbol{r_1}$ to position $\boldsymbol{r_2}$, that satisfies the initial boundary condition $P(\boldsymbol{r_2}, T_D = 0) = f_\delta(\boldsymbol{r_2} - \boldsymbol{r_1})$, can be modeled with a Gaussian distribution function according to

$$P(\boldsymbol{r}, T_D) = \left(\frac{1}{\sqrt{4\pi D T_D}}\right)^3 \cdot \exp\left(\frac{-\boldsymbol{r}^2}{4DT_D}\right) \qquad \text{Eq. 2}$$

where T_D is the observation time and f_δ denotes the Dirac delta function.

In an n-dimensional macroscopic system freely diffusing particles, initially concentrated to a point, would disperse in a radial manner with a root mean square displacement $\langle \boldsymbol{r}^2 \rangle$ related to the diffusion coefficient according to $\langle \boldsymbol{r}^2 \rangle = 2nDT_D$.

2.3 Modeling anisotropic diffusion

To describe directionally dependent diffusion the scalar diffusion coefficient D must be replaced with a more complex metric. One of the available models, and one of the simplest ones, is the diffusion tensor model which is the basis of DTI [13].

Using the diffusion tensor $\boldsymbol{D}$, which is a second order tensor according to Eq. 3, means keeping the Gaussian probability function as a model for the translation, but it lets the variance of the Gaussian function vary in different spatial directions.

$$\boldsymbol{D} = \begin{bmatrix} D_{xx} & D_{xy} & D_{xz} \\ D_{yx} & D_{yy} & D_{yz} \\ D_{zx} & D_{zy} & D_{zz} \end{bmatrix} \qquad \text{Eq. 3}$$

The diffusion tensor can be represented geometrically by a diffusion ellipsoid where the surface shows the isobar displacement distribution.

This tensor is rotationally invariant, *i.e.* $D_{ij} = D_{ji}$, and can thus be described by only six unique elements.

By diagonalizing the diffusion tensor, *i.e.* transform the coordinate system to coincide with the principal directions of the ellipsoid rather than using the magnet coordinate system, the diffusion tensor can be described by its eigenvalues. The largest eigenvalue λ_1 is called the principal eigenvalue, followed by λ_2 and λ_3 in order of decreasing magnitude. These are depicted together with the ellipsoid isobar surface in Figure 2.

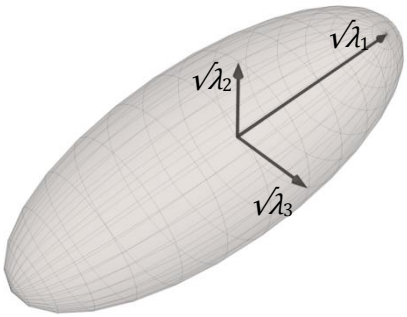

Figure 2 – Graphical representation of anisotropic diffusion according to the diffusion tensor model. Particles originating from the center of the ellipsoid have the same probability to end up anywhere along the surface after a given diffusion time. Seeing how the particle has an equal probability to end up far away from its origin in the direction of λ_1 and stay close to the origin in the direction of λ_2 and λ_3 it appears that the diffusion has a preferred direction along λ_1.

These eigenvalues can be used for evaluation, as are, or be combined to create other, more tangible, diffusion indices. Commonly used indices include the mean diffusivity (MD), the axial diffusivity (D_{axi}), the radial diffusivity (D_{rad}) and the fractional anisotropy (FA), according to

$$MD = \frac{\lambda_1 + \lambda_2 + \lambda_3}{3} \quad \text{Eq. 4}$$

$$D_{axi} = \lambda_1 \quad \text{Eq. 5}$$

$$D_{rad} = \frac{\lambda_2 + \lambda_3}{2} \quad \text{Eq. 6}$$

$$FA = \left(\frac{3}{2} \cdot \frac{\left(\lambda_1 - \overline{\lambda}\right)^2 + \left(\lambda_2 - \overline{\lambda}\right)^2 + \left(\lambda_3 - \overline{\lambda}\right)^2}{(\lambda_1^2 + \lambda_2^2 + \lambda_3^2)} \right)^{1/2} \quad \text{Eq. 7}$$

where $\overline{\lambda}$ is the mean of all three eigenvalues.

2.4 The diffusion imaging pulse sequence

The standard diffusion weighted sequence is a once-refocused pulsed-gradient spin-echo (PGSE) with two diffusion encoding gradients [36], as depicted in Figure 3.

The basic principle of diffusion sensitization is to create a sequence that provokes signal attenuation related to the net particle movement. This is done as follows: The first pulsed gradient (A.) produces a phase shift along the gradient direction. The spins then continue to de-phase, through T2-relaxation, as well as diffuse through the medium. The de-phasing is then reverted by the 180° pulse, refocusing the spins. The second gradient pulse (B.) then introduces another phase shift, in the opposite direction to A., effectively returning the system to its original state accounting for all but the movement experienced by the particles between the two pulsed gradients. Thus the net movement along the gradient direction results in signal attenuation caused by incomplete refocusing [34].

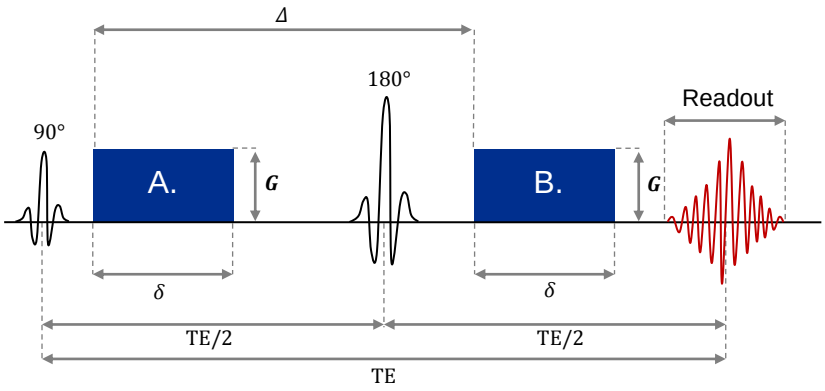

Figure 3 – Schematic pulsed-gradient spin-echo sequence. The sequence is a standard spin echo sequence with two additional diffusion sensitizing pulsed gradients (A. and B.). Note that the two pulsed gradients A. and B. are of the same polarity but work to restore the net phase shift because they are separated by a 180° refocusing pulse.

The signal expression can be derived from the phase shift of the spin ϕ as a function of the translation vector $\boldsymbol{r} = (\boldsymbol{r_2} - \boldsymbol{r_1})$, the gradient duration δ and the gradient vector $\boldsymbol{G}$ according to

$$\phi = \gamma \cdot \delta \cdot \boldsymbol{G} \cdot \boldsymbol{r} \qquad \text{Eq. 8}$$

where γ is the proton gyromagnetic ratio.

The diffusion weighted signal S can be written as

$$S = S_0 \int P(\phi, T_D) \cdot e^{i\phi} d\phi \qquad \text{Eq. 9}$$

where $P(\phi, T_D)$ is the probability distribution function of the phase shift, T_D is the effective diffusion time [37] approximated by $T_D = \Delta - \delta/3$ to compensate for the fact that the pulsed gradients are not instantaneous [35] and S_0 is the signal in the absence of

a diffusion encoding gradient, also known as b0 signal. Substituting the phase shift for the translation according to Eq. 8 gives S according to

$$S = S_0 \int P(\boldsymbol{r}, T_D) \cdot e^{i\gamma\delta \boldsymbol{G}\boldsymbol{r}} d\boldsymbol{r} \qquad \text{Eq. 10}$$

Assuming that the propagator is a Gaussian according to Eq. 2 the expression is the Fourier transform of the propagator according to

$$FT[\langle P(\boldsymbol{r}, \mathrm{T_D})\rangle] = S_0 \int P(\boldsymbol{r}, T_D) \cdot e^{i\gamma\delta \boldsymbol{G}\boldsymbol{r}} d\boldsymbol{r} \qquad \text{Eq. 11}$$

which is analogous to the signal in the diffusion weighted images. The standard solution to this integral gives the signal as a function of $\boldsymbol{b}$ according to

$$S(b) = S_0 \cdot e^{-bD} \qquad \text{Eq. 12}$$

where $b = \gamma^2\delta^2G^2T_D$, see [34] for complete derivation.

By collecting the signal in each voxel as a function of the varying spatial direction of the pulsed gradient we can fit the DTI model to the measured data, creating a tensor like the one in Figure 2.

The diffusion coefficient measured this way is often called the apparent diffusion coefficient (ADC) owing to the fact that it is not a measure of the intrinsic diffusion but rather a diffusion coefficient affected by the interactions between the diffusing medium and its surrounding [1].

2.5 Streamline tractography

A tractography, or tractogram, is the graphical representation of the directionality in a tensor or vector field. There is a wide variety of tractography algorithms that can be used to visualize, for example diffusion, blood flow or CSF pulsation. The two main types of tractography are based on local vector information and global energy minimization algorithms respectively. Only the interpolated streamline algorithm, used in this work, will be explained due to the limited scope of this work.

The interpolated streamline is a deterministic line propagation algorithm based on local vector information. It is mathematically defined as a trajectory propagating parallel to the vector field in its proximity. In DTI it creates a tract in 3D space that is parallel to the tensor field principal eigenvalue. Because the DTI tensor field is discrete it is interpolated to make the tract line derivative continuous [38], meaning that the line propagation will not only be based on the voxel that it inhabits but will also draw directional information from neighboring voxels, as seen in Figure 4.

Tractography is controlled by predefining a number of tracking parameters. These are primarily criteria determining where to seed and when to terminate a track. Seeding can be defined with respect to any available image contrast using simple signal value

thresholding. Track termination can be based on parameter map values, much like the seeding, but can also include tracking angle restrictions [2, 38].

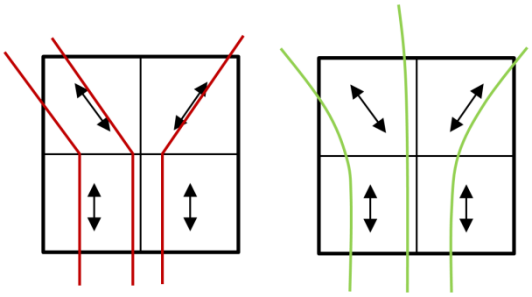

Figure 4 – Schematic examples of non-interpolated (red lines) and interpolated streamline (green lines) tracking in the same 2D vector field (black squares and arrows). The figure is adapted from [38].

Using the FA map thresholding is an effective way to seed in the regions where there is high diffusion directionality, usually associated with WM. It also serves as an effective termination criteria eliminating tracks entering CSF where the FA is low. Parameters like track angle and track length thresholding can be adjusted to benefit specific structures. With this in mind it should be beneficial to use low track angle and high track length thresholds when examining the spine due to its oblong structure. Looking at the distorted tractography in Figure 5 it is obvious that the use of length thresholding is limited if the spinal tract structure contains short, misaligned, segments. Performing tract length thresholding in this case would produce so called "gaps", excluding sizable parts of the spinal volume from the segmentation.

Before evaluating DTI tractography it is advisable to familiarize oneself with the limits of DTI and to understand that the tracts in a tractogram are not direct representations of nerve fibers and are not implicit proof of actual axon connections but are rather mathematical representations of local diffusion anisotropy as described by the DT model.

2.6 Image distortion

The readout technique most commonly used in diffusion measurements is echo planar imaging (EPI) [17]. Its usefulness comes from its speed, *i.e.* ability to sample the entire k-space in one echo, effectively avoiding issues with intra-echo subject movement and allowing a high number of diffusion directions in a feasible acquisition time. Its drawback is that it has a limited bandwidth in the phase encoding direction, making it sensitive to field inhomogeneity, eddy-currents (EC) and physiological movement [17, 39].

When using rapidly switching gradients EC are induced in conductive materials within the MRI scanner. These currents give rise to unwanted magnetic field perturbations that stretch or compress the image in proportion to the encoding gradient amplitude [3] and are different in all diffusion encoding directions [40]. This problem is

especially pronounced in DTI because the pulsed gradients are temporally drawn out separating the incline and decline of the pulsed gradients removing the self-compensating effect that usually negates the EC [3, 40].

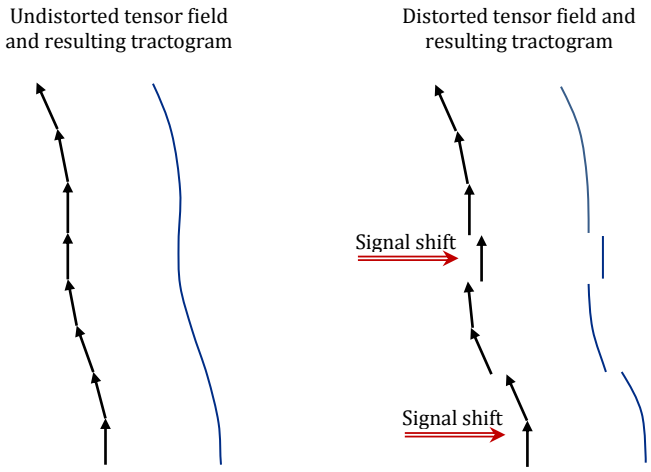

Figure 5 – Schematic depiction showing that the signal shift (red arrows), caused by susceptibility differences along the spine, causes the tractography (blue line) to fragment where the tensor field (black arrows) is no longer properly aligned. Note that the signal shift is directed in the phase encoding direction, in this example it is the RL direction.

EC can be prevented by active shielding and altering the employed gradients to include compensation for the EC [41]. It can also be corrected post-hoc with methods such as dynamic field correction using the b0 image as a reference [42].

The distortions due to local field inhomogeneity are caused by susceptibility differences in the tissues surrounding the spinal canal, owing mostly to the air-tissue interfaces at the esophagus and lunges as well as the spinal column [40]. This distortion can be seen as a signal shift in the phase encoding direction or signal intensity change due to many-to-one mapping [3]. In the distorted areas the signal phase shift ϕ is proportional to the local off-resonance frequency ω according to

$$\phi = 2\pi\omega \cdot (t - TE) \qquad \text{Eq. 13}$$

where TE is the echo time and t is the readout time. Including this off-resonance effect in the signal function $S(t)$ it can be seen how it adds a shift y_{shift} in the phase encoding direction according to

$$\begin{aligned} S(t) &= \int f(x,y) \cdot e^{2\pi i\omega(t-TE)} \cdot e^{2\pi i(k_x x + k_y y)} dx\, dy \\ &= \int f(x,y) \cdot e^{2\pi i\left(k_x x + k_y\left(y + y_{shift}\right)\right)} dx\, dy \end{aligned} \qquad \text{Eq. 14}$$

where the average read-out speed r, in the k_y direction, has been approximated by $k_y/(t - TE)$ [40].

In DTI the distortion has roughly the same effect in all diffusion encoding directions, as it is mainly caused by inhomogeneity in the main magnetic field. This means that even though signal is shifted it is still traceable to its correct anatomical origin. Thus it is not strictly necessary to correct for this distortion before calculating the diffusion parameters. Although evaluation of diffusion parameters is possible without correction a significant problem arises when trying to use the tractogram created from uncorrected data. As seen in Figure 5 the signal shift does not change the tensor orientation in each voxel but it disrupts the tensor field alignment making it harder to perform a valid tracking, as described in 2.5.

3 Materials and Methods

3.1 MRI system

All imaging was performed on a Siemens MAGNETOM Skyra (3 T) at the Lund University Hospital. The camera has a 70 cm bore diameter and a gradient system capable of 45 mT/m and a slew rate of 200 T/m/s.

The coils used were the 20 channel "Head/Neck 20" and the 32 channel "Spine 32" using only the elements relevant to the applied FOV.

3.2 DTI phantom

A synthetic phantom was constructed to facilitate DTI in a simple and static geometry. It was constructed according to an in-house developed method based on the fiber material choice presented by Fillard et. al [43]. The geometry of this phantom was chosen to resemble the cervical spinal cord with respect to length and circumference.

The phantom, seen in Figure 6, is composed of MR compatible materials including a cylindrical shell, three guide-rods and four fiber bundles. The fiber bundles are composed of an acrylic-fiber core (100 %) tightly enclosed in plastic tubing.

The fiber bundles were produced by aligning acrylic yarn in loose bundles and submerging them in water to drive out the air. To ensure that as little air as possible was remaining after submersion the fibers were boiled several times. While still under water the bundles were inserted into shrinking tube to compress them into tightly packed rods. After the application of shrinking tube the bundles were boiled again. This boiling ensures that the gasses still trapped in the bundle expand and are evacuated along with the steam created in the boiling process; any remaining pockets of air and steam are expected to be reabsorbed by the liquid when it is allowed to cool.

For the phantom to be compatible with the quantitative evaluation plastic landmarks, visible in TSE and b0 images, were fixated along the length of the cord to define two outer points of the primary cord (top and bottom). The distance between the top and bottom markers is 18 cm.

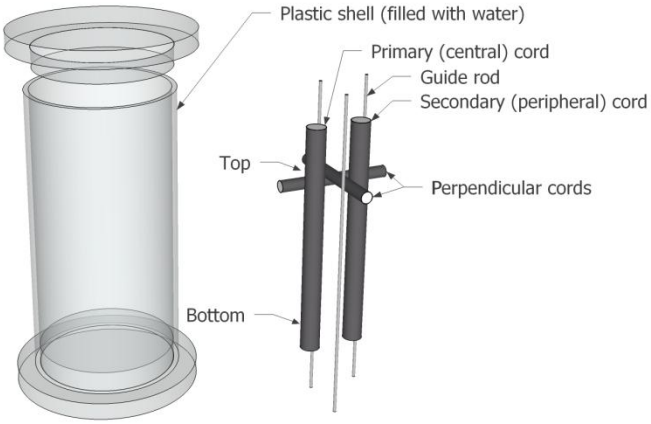

Figure 6 – DTI phantom model. Attached to the guide rods are two main cords, each with a diameter and length of roughly 14 mm and 250 mm respectively. At the top there are two small perpendicular rods. The central cord is roughly coaxial with the outer shell and is referred to as the "primary cord". The remaining two cords are supplementary to the primary cord and are used for internal reference.

3.3 Acquisition design

The imaging protocol, acquisition parameters and surrounding methodology was developed in parallel with the validation and testing of the system. Unless stated otherwise, the sequence parameters and imaging geometry featured in this section was used for subsequent investigations.

3.3.1 Imaging protocol

The imaging protocol is composed of three separate imaging series including the DTI, an anatomical reference imaging series and a high resolution anatomical series, resulting in a total acquisition time of 5 minutes.

The DTI is performed with diffusion sensitized single shot echo planar imaging (SSEPI) using 64 non co-linear diffusion gradient directions (NDGD) employing *b*-values of 0 and 800 s/mm^2, with a spatial resolution of 2.0×2.0×2.0 mm^3, utilizing an EPI readout. The image volume is comprised from 13 contiguous sagittal slices with an anteroposterior phase-encoding direction. A more detailed parameter list is featured in Table 1. Beyond these parameters it is also beneficial to engage fat saturation to reduce fat artifacts; dynamic field correction (DFC) to correct for EC; field shimming to reduce inhomogeneity artifacts; and parallel imaging to reduce acquisition time. For this protocol these were chosen as follows: fat saturation "Strong", dynamic field correction "Direct", shim mode "Standard" and the parallel imaging acceleration factor is 3.

The reference series is a turbo spin echo (TSE) acquired with the same FOV, resolution and TE as the DTI series to facilitate the geometrical distortion correction of data as detailed in 3.4.2.

The high resolution anatomical series is a sagittal T2-weighted series with the same FOV as the DTI but with a spatial in-plane resolution of 0.8×0.8 mm² and a slice thickness of 2 mm.

Table 1 – Sequence parameters used in the standard DTI protocol

Parameter	Value
TE	63 ms
TR	2300 ms
Bandwidth	1954 Hz/pixel
Voxel size	2 x 2 x 2 mm³
FOV	256 x 256 x 26 mm³
b-Value	0 and 800 s/mm²
Partial Fourier	6/8
Number of b0 images	1
NDGD	64
iPAT/GRAPPA	3
Correction techniques	DFC
Acquisition time	2 min 43 sec

3.3.2 Subject positioning and imaging geometry

Subjects are placed in the MRI scanner in a head first supine (HFS) position taking special care not to tilt the head backwards preventing unnecessary curving of the spine in the sagittal plane.

Scout images, like those seen in Figure 7, are used to position the FOV over the cervical spine, ensuring that the entire structure, from pons to the first thoracic vertebrae is included. A 50 mm saturation band is placed over the face and anterior part of the torso to prevent signal disturbance from the mouth, esophagus and chest. A manual shimming volume is defined over the spinal canal to increase field homogeneity in the region of interest.

The DTI phantom was placed in the scanner in a geometry that mimics the scanning position of the human spine as closely as possible. This means placing the phantom primary cord in the very center of the head coil and adjusting its location along the couch so that the cord covers the same area as the cervical spine with respect to the receiving coils. Positioning the FOV, adjustment volume and saturation band is done as if it were an *in vivo* experiment.

Before any DTI measurement were performed the phantom was left at rest for a minimum of 10 minutes to make sure that no bulk movement was present in the free water volume.

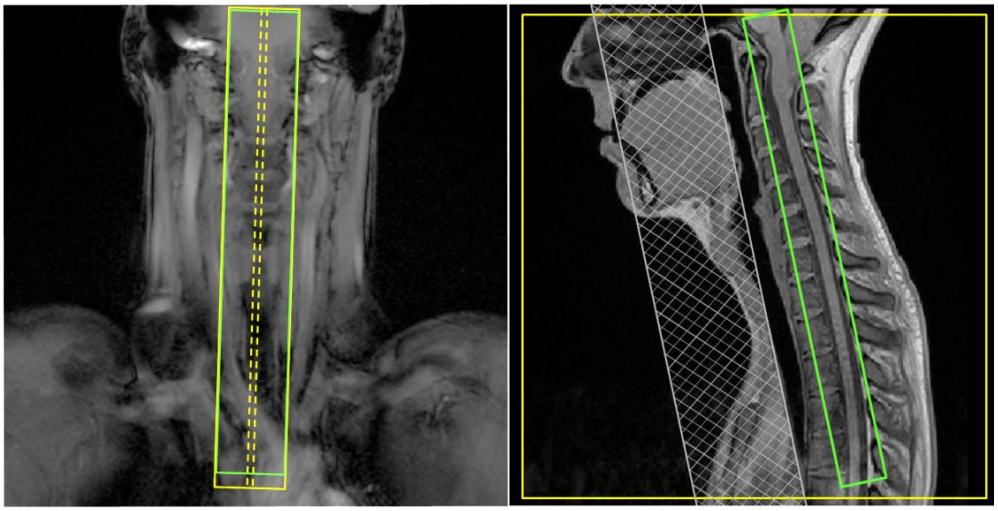

Figure 7 – Coronal (left) and sagittal (right) scout images showing desired positioning of FOV (yellow), adjustment volume (green) and saturation band (checkered gray). The phase encoding is directed along the patient AP direction. It should be noted that this subject has a relatively straight spine making the position of the adjustment volume easy. In case of a more undulating spinal structure the adjustment volume was decreased in the IS direction, prioritizing the inclusion of the seven cervical vertebrae.

3.4 Data processing

Data processing was designed to utilize as much of the existent infrastructure as possible to minimize the need for custom development. Custom programs were used mainly to interface third party software and to perform necessary corrections.

The process of data evaluation can be divided into three key components: parameter reconstruction, distortion correction and quantification. These three parts are schematically depicted in a flow chart in Figure 8 and described in more detail in the paragraphs below.

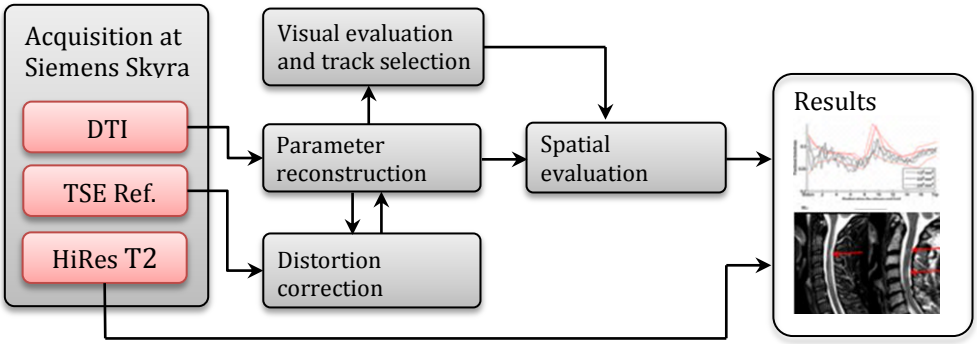

Figure 8 – Data flowchart depicting the processing of the three acquired image series. Each red box represents a set of image data and grey boxes represents a program or software framework. Note that it is possible to completely bypass the correction step to evaluate uncorrected data. In this case the TSE reference series are not used.

3.4.1 Diffusion tensor and parameter map reconstruction

The third party software package Diffusion Toolkit [44] and TrackVis [45] were used for the reconstruction and visualization of the diffusion tensor field and the diffusion parameter maps respectively.

Parameter calculation, reconstruction, and tracking was performed on data without the use of smoothing, subject movement correction or EC correction other than the DFC. Track seeding was done on the FA map with a threshold of 0.2 and 0.1 for *in vivo* and phantom experiments respectively. Each seeded voxel was set to contain two randomly placed seeds within its volume. The tracking was performed with an interpolated streamline algorithm where the angular threshold was set to 20° and track spline filtering was engaged.

Track selection was performed by discarding all tracks shorter than 60 mm. In the event of any disturbing tracks still remaining, such as those created in fat tissue, these were manually removed by ROI exclusion.

The tractography results were visually inspected in TrackVis to ensure that no gross error had occurred during reconstruction or in the subsequent geometrical distortion correction. The results were also checked to ensure that no gaps, as described in Figure 5, were remaining.

3.4.2 Geometrical distortion correction

To improve the functionality of the tractography based segmentation, in this case specifically the track length thresholding, the data was corrected for the geometrical distortions introduced by the field inhomogeneity, as explained in 2.6.

The correction was performed using the in-house program "Geometrical Distortion Correction" (GDC) developed in the Matlab framework (Mathworks, Natick, MA, USA) specifically for this project.

The signal shift estimation is based on the comparison of spinal geometry in the TSE reference series, that is assumed to be distortion-free, and the DTI b0-weighted images. The reference and b0 images were resampled in transversal slices, then co-registered by matching the signal intensity from the spinal tract using a rigid 2D iterative sum of squares matching algorithm much like the one described by Wu *et al.* [46]. The shift resulting in an optimal image match is stored in what is called the "correction vector". To stabilize the matching procedure the images are masked by manually defining a polygonal area corresponding to the spine using basic ROI definition tools on the central sagittal slice.

Once the distortion has been estimated, the axial slices of the parameter maps are shifted in the anteroposterior direction according to the information stored in the correction vector. The same shift is also performed on the tensor field.

After implementing the GDC a second tractography is performed using the corrected tensor field, together with the corrected parameter maps, this data is used for all further evaluation.

Note that no correction was performed on data acquired in the phantom owing to the small influence of susceptibility artifacts.

3.4.3 Spatial quantification of DTI parameters

Evaluation of DTI parameters along the spinal tract was performed in the in-house developed program "Quantitative Tractography Evaluation" (QuTE) [47, 48].

QuTE uses the selected tracks, from a given structure, to calculate a single mean-track that is a representation of all the initial tracks. For a given spacing, QuTE then projects all of the DTI parameters, from a plane perpendicular to the track, onto the mean-track, creating a one dimensional parameter vector. This information can now be plotted as a function of the position along the mean-track. By defining anatomical reference points along the mean-track, so called landmarks, QuTE co-registers the DTI parameter information from several subjects so that they can be compared with respect to the same anatomical location.

Seven landmarks were manually placed in the TSE and b0 image volumes to define the spinal structure relative to the mean-track.

The first landmark was set to the superior part of the first cervical vertebrae (C1) and the rest were set at the level of the disks separating the vertebrae, spanning from the inferior part of the second cervical (C2) vertebrae to the inferior part of the seventh cervical vertebrae (C7), as seen in Figure 9. Due to the complex structure of the first and second vertebrae these were treated as one segment.

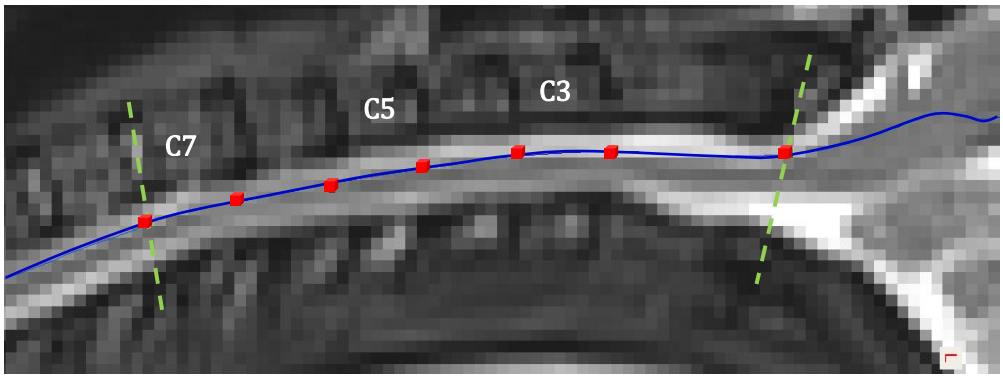

Figure 9 – Landmarks (red voxels) placed in a TSE reference image volume together with the mean-track (blue line). Note that the backdrop-image is an off-center sagittal slice and that the mean-track as well as the landmarks have been intensified to make these features more visible. The dashed green lines show schematic examples of how the most inferior and superior landmarks were placed with respect to the reference image.

In the *in vivo* pilot study diffusion tensor indices from the normal material were compounded into a plot showing the normal group mean of any given metric as a function of anatomical position along the spine. To include the variance in these metrics the plot also contains lines showing two standard deviations from the normal group mean.

By superimposing individual patient data onto the same diagram we compare patient specific DTI parameters to the normal material as a function of anatomical position.

In addition, visual evaluation of the high resolution T2-weighted images was performed by a radiologist to confirm or denounce the presence of MS lesions in the cervical spine.

3.5 System validation

To ensure optimal image quality and to evaluate acquisition parameter choices, extensive quality control and validation was performed parallel to the evolution of the DTI acquisition protocol. This was necessary since DTI-specific quality controls were not performed at this scanner, and were, to some extent, not possible before the introduction of the synthetic DTI phantom.

The quality control and validation included: data acquisition with respect to parameter tuning, coil selection as well as subject positioning and image geometry; implemented software modalities such as field correction techniques, field adjustment and saturation band placement; data transfer and pre-processing with respect to data integrity such as the correct preservation of tensor orientation and b-matrix interpretation; parameter map calculation and reconstruction; and post-processing including the geometrical distortion correction and parameter quantification.

Some of the most important and interesting validation experiments are described below.

3.5.1 Spatial dependency

Spatial dependency was evaluated to test the hypothesis that there was an influence on the DTI metrics from imperfections in the MRI scanner, specifically the gradient system.

The experiment was performed using a ROI based and a tractography based evaluation. In the ROI based method the free water volume (*i.e.* outside any fiber bundle) was used to calculate the MD and FA in 10 equidistant ROI alongside the primary cord. In the tractography based method standard evaluation of MD and FA was performed on the primary cord.

3.5.2 Signal to noise ratio

The SNR is known to affect the resulting DTI metrics [3, 49] and is, for example, dependent on the receiver coil sensitivity in the image volume. This is especially important in the case of imaging of the spine as the FOV spans over two separate coils which could impact the SNR homogeneity effectively biasing any parameter evaluation.

SNR dependency on signal origin relative to the receiver coils was studied along the IS direction. SNR maps were produced for five consecutive phantom and *in vivo* measurements and plotted as a function of phantom cord and spine position. The SNR was estimated in all image volume voxels by dividing the b0 image signal by the signal variance estimated from the tensor model fit residual.

Standard evaluation was performed and SNR plots as a function of position were compared.

3.5.3 Reproducibility

To evaluate the system stability with respect to initial data acquisition as well as the subsequent post-processing a reproducibility experiment was performed.

Five consecutive DTI measurements were performed on one volunteer without having the volunteer exiting the scanner between acquisitions. Standard evaluation was performed on the five datasets using the same reference image series for the GDC.

To investigate the function of the GDC the five correction vectors were plotted and compared to evaluate any discrepancies in the distortion correction algorithm.

3.5.4 Geometrical distortion correction

The hypothesis that the tractography benefitted from the GDC was tested by comparing corrected vs. uncorrected data. In the absence of a golden standard for comparing tractography the author performed a quantitative test combined with qualitative visual observation.

In the quantitative test the amount of generated tracks surpassing a certain length was used as a quality measure, where a larger amount of long tracks was indicative of better quality. The ratio of tracks before and after correction was compared for each volunteer for length thresholding at 60 and 100 mm.

Visual inspection was focused on detecting gaps in the tracking of the spinal cord at the standard length thresholding of 60 mm for volunteer and patient data. It was also used to determine if the coherence of spinal track geometry to reference spinal anatomy in the cervical spine was improved or deteriorated by the GDC.

3.6 In vivo pilot study

To evaluate the functionality of the evaluation method as a whole as well as the ability of the suggested DTI to detect tissue changes due to MS a comparison of healthy volunteers and MS patients was performed.

Normal material was collected from invited volunteers where the prerequisites for entering the study were that the volunteer did not suffer from any known injury of the spinal cord.

Patients suffering from MS were selected from those currently being treated or diagnosed at the Lund University Hospital. Selection was done by an experienced radiologist. The normal material consisted of eleven volunteers (five female and six male) between the age of 24 and 60 (the mean age was 39). The patients were two women, ages 35 (Patient A.) and 65 (Patient B).

The study was approved by the local ethics board and all participants signed an informed consent form.

Datasets were excluded in case of the following:

- Spinal tract was not completely enclosed by the FOV from pons to the inferior side of the seventh cervical vertebrae
- Subject movement prevented data to be correctly evaluated
- Tractography could not be performed under predefined conditions
- Anatomical images showed pathology or damage (not applied for MS patients).

4 Results

Presented results are divided into validation and pilot study oriented findings. The focus of the validation results is to illuminate some of the technical aspects and details of this particular method while the *in vivo* pilot study results are a product of the entire method spanning all of its aspects. It is important to note that these tests were performed in parallel with the pilot study and in some cases validation results are based on data collected in the *in vivo* study.

4.1 System validation

4.1.1 Spatial dependency

A ROI based and tractography based evaluation of the spatial dependency was performed in the free water volume as well as in the primary cord of the phantom.

As seen in Figure 10, a dependency on spatial position exists along the IS axis for MD as well as the FA. Across the 18 cm of the phantom primary cord the MD max/min ratio was in the order of 10 %, it is also seen that the FA is more biased at the peripheral parts of the volume. There is also an indication that the variation across a longer segment would be larger.

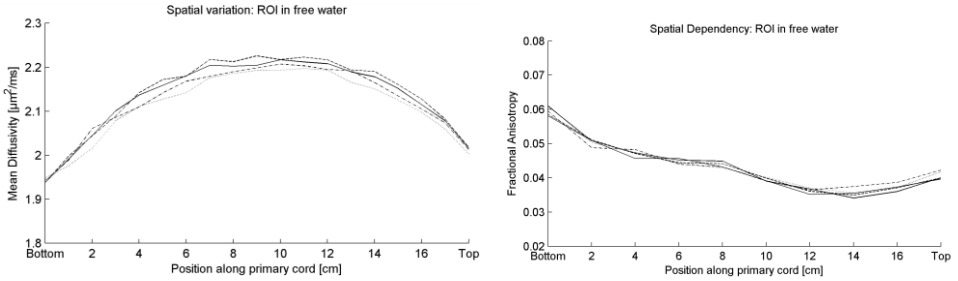

Figure 10 – Calculated MD (left) and FA (right) in the free water volume of the phantom using the ROI method. A peak MD of 2.2 $\mu m^2/ms$ was measured at the location of the phantom center which coincides roughly with the isocenter of the scanner. Each line represents one DTI series. The experiment shows MD dependency on position along the primary cord and the FA diagram indicates that the error can be directionally variant.

The tractography based experiment presented in Figure 11 shows that the MD and FA in the phantom primary cord exhibit a spatial dependency. The MD is concave as a function of position, much like the result in the free water volume, and the FA exhibits a convex dependency. Note that the decrease in MD and increase of FA at the

center of the cord is indicative of an unintentional constructional flaw possibly due to harder fiber compression at this location.

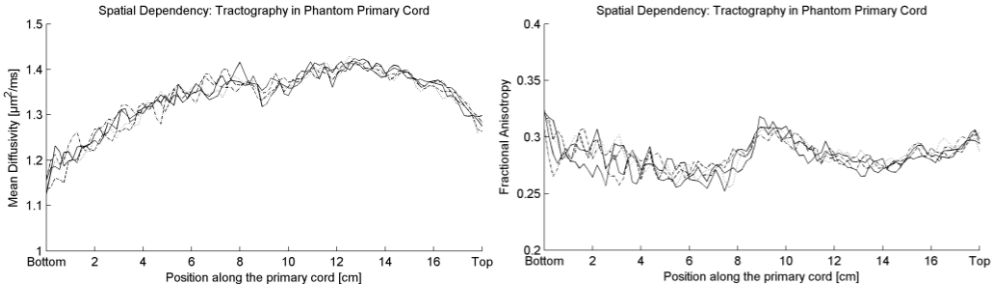

Figure 11 – Calculated MD (left) and FA (right) in the phantom primary cord using the tractography method. Each line represents one DTI series. The MD exhibits a spatial dependency similar to the one in Figure 10. The FA exhibits a dependency that could be an effect of the directionally dependent influence on the diffusivity shown in Figure 10. Note that the central part of the cord has a decreased MD and increased FA possibly due to excessive compaction of the fibers in this region.

4.1.2 Signal to noise ratio

The SNR as a function of position along the phantom primary cord and volunteer spinal cord is shown in Figure 12.

The phantom experiment clearly shows that there is an effect on the SNR with respect to the position along the cord, where more inferior parts suffer from lower SNR.

The *in vivo* data shows a greater variability compared to the phantom and although there is an indication of the SNR being slightly higher in the superior direction it is not strictly decreasing for more inferior positions.

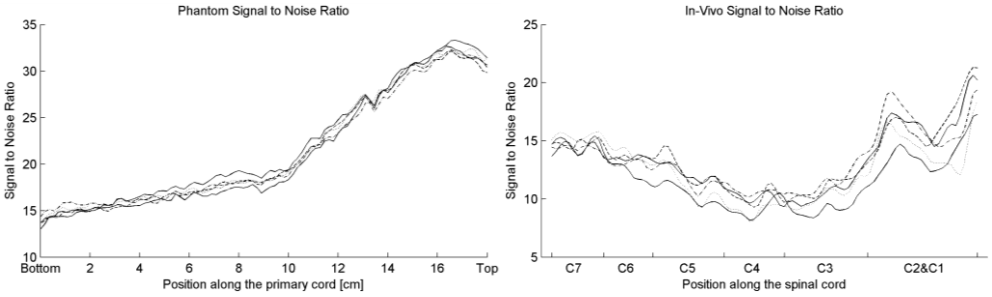

Figure 12 – Five consecutive SNR measurements in phantom (left) and *in vivo* (right) plotted as a function of primary cord position and along the spinal cord. The phantom shows a high SNR in the top region where the cord is the furthest inside the head coil. As the signal originates further away from the head coil the SNR is consistently lowered. The *in vivo* case has a more complicated pattern exhibiting the lowest SNR at the level of C4 and C3 although still having the highest SNR for the most superior parts of the spinal cord.

4.1.3 Reproducibility

Figure 13 shows MD and FA for five consecutive *in vivo* measurements. The reproducibility can be gauged from the parameter plot coherency or the error bars in the

segmented plot. It varies depending on position along the spine and is in the order of 10 to 20 %.

Figure 14 shows the correction vector corresponding to each one of the five acquisitions. The maximal shift was roughly 4 mm, found in the region corresponding to the last cervical and first thoracic vertebrae. The largest variation of correction can be found at the level of the first and second cervical vertebrae where the most extreme corrections vary in the range of 4 mm.

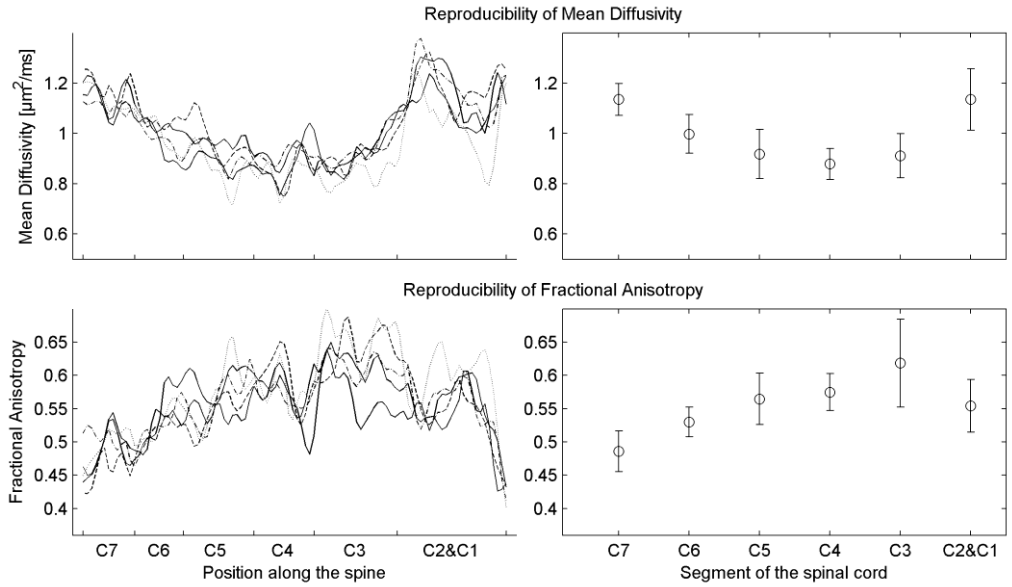

Figure 13 – Five FA and MD curves acquired from the same subject plotted as a continuous function of anatomical position along the spine (left side) and the same data condensed to segments of the spine (right side). The error bars show two standard deviations from the mean value in each segment.

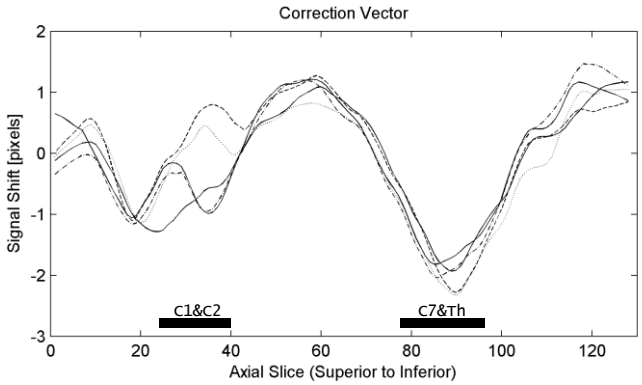

Figure 14 – The five lines show the resulting correction vector in the reproducibility experiment. The signal shift is given in pixel units where each pixel corresponds to 2 mm. The x-axis is likewise defined as the number of axial slices from the most superior part of the FOV where each slice has a thickness of 2 mm. The rectangles mark out specific anatomical regions.

4.1.4 Geometrical distortion correction

Quantitative and qualitative tests were performed on the *in vivo* data to evaluate the effect of the GDC on the end result. The total number of tracks comparison showed that the mean number of tracks remaining after GDC was 46 % higher for thresholding at 60 mm and 196 % higher for thresholding at 100 mm.

The visual evaluation showed that all, except one, of the uncorrected tractograms had at least one visible gap in the inferior region of the cervical spine. In addition, two of the volunteers had significant gaps at the level of the pons and superior part of C1 respectively. After the GDC only one gap in the cervical spine remained although it was made significantly smaller allowing for it to be processed. The gaps found at the level of the pons and C1 remained even after correction, though the first mentioned was processed because the tracking failed outside the region of interest. The visual control also concluded that all sets of data had tractograms that corresponded as well, or better, to the reference image anatomy after the GDC.

Examples that show generally representative tractographies, before and after GDC, are shown in Figure 15 and Figure 16.

The GDC did show signs of sub-optimal correction. Figure 17 shows sharp edges in the tractography implying that the tensor field is not in optimal alignment.

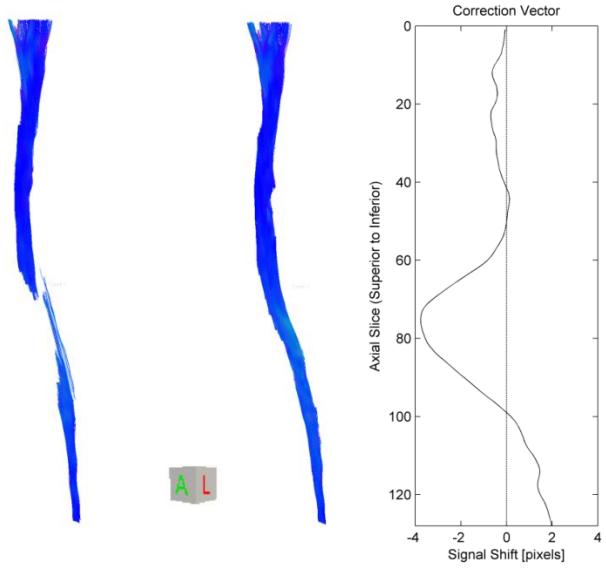

Figure 15 – Two tractograms from the same subject show the difference before (left) and after (center) GDC as well as the correction vector for this particular case (right). Both tractograms were generated using the same reconstruction parameters and a track length thresholding excluding all tracks shorter than 60 mm. The uncorrected result has a large gap in the tract structure at the level of the sixth and seventh cervical vertebrae. This gap was effectively removed by the GDC by applying a pixel shift according to the correction vector. The correction vector is plotted in roughly the same scale as the tractograms to illustrate the shift that was introduced by the GDC. Negative values of the correction vector produce a shift in the anterior direction.

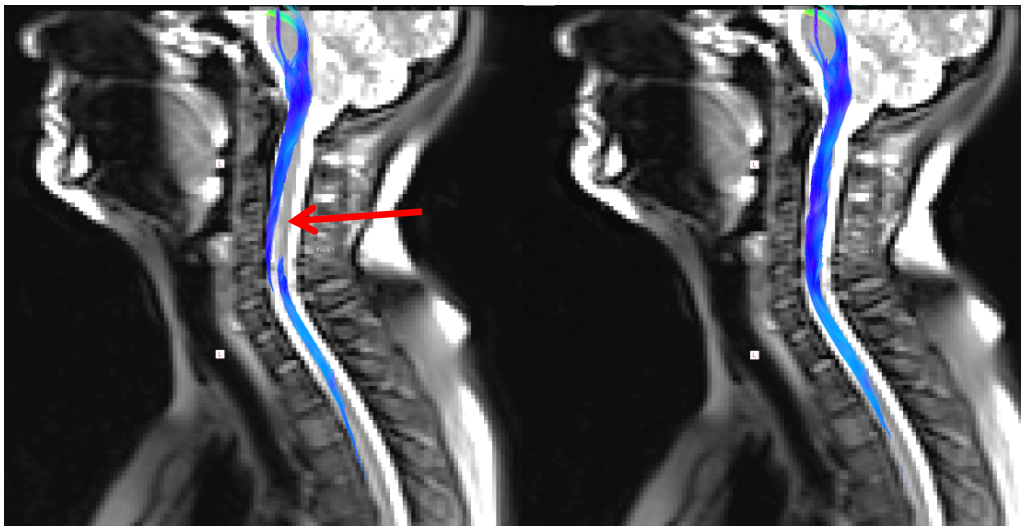

Figure 16 – Uncorrected (left) and corrected (right) tractograms superimposed on a sagittal TSE reference image. The uncorrected image shows a large discrepancy (red arrow) between the tracts and the anatomical position of the spine in the reference image. After the GDC this discrepancy can no longer be seen. Note that, in this case, the tracking fails below the level of the second thoracic vertebrae.

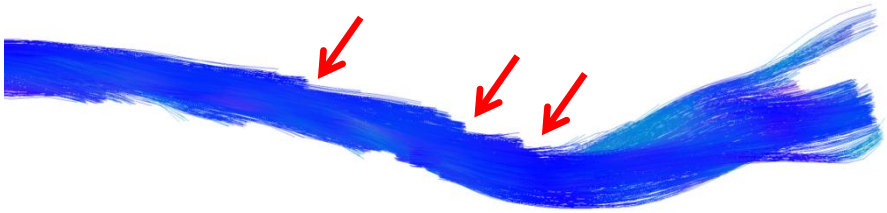

Figure 17 – Tractography of the spine. Left to right in the figure is inferior to superior covering a span from C4 to the pons. The red arrows point to some of the abrupt breaks in the tractography indicating sub-optimal tensor field alignment.

4.2 In vivo pilot study

The standard DTI protocol and evaluation was implemented to study the cervical spine of eleven healthy volunteers and two MS patients. One set of data was excluded due to incomplete tracking at the level of the first cervical vertebrae.

High resolution T2-weighted images acquired in this study as well as in prior diagnostic images were evaluated to locate MS-lesions in the cervical spine of the patients. Figure 18 shows two high resolution T2-weighted images of the cervical spine in both patients. Radiologist evaluation concluded that Patient A. had a strong indication of a diffuse spinal lesion located at the level of C2-C3. Patient B. had confirmed lesions at the level of C2-C3, C4 and several other diffuse lesions throughout the inferior half of the cervical spine.

Figure 19 shows the resulting volunteer and patient DTI metrics. On the left the parameters are presented as a function of anatomical position and on the right the same parameters are compounded into segment specific values. It should be noted that even though GM has a relatively low FA compared to WM [4, 22] it was not excluded by the tractography but produced complete tracking much like the WM.

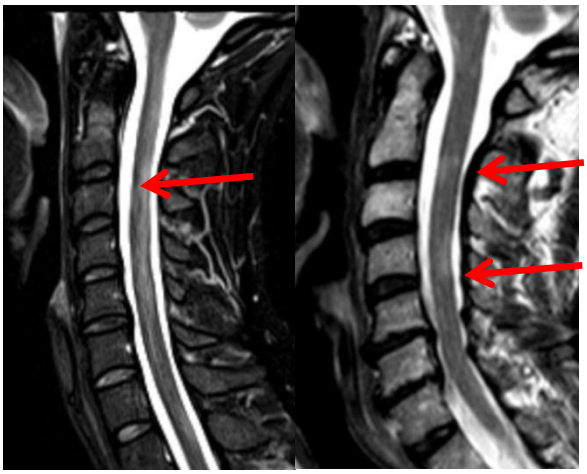

Figure 18 – High resolution T2-weighted sagittal images of the two patient spinal cords. Patient A. (left) had a suspected diffuse lesion at the level of C2-C3 and Patient B. (right) had several confirmed lesions at the level of C2-C3 and C4 as indicated by the arrows.

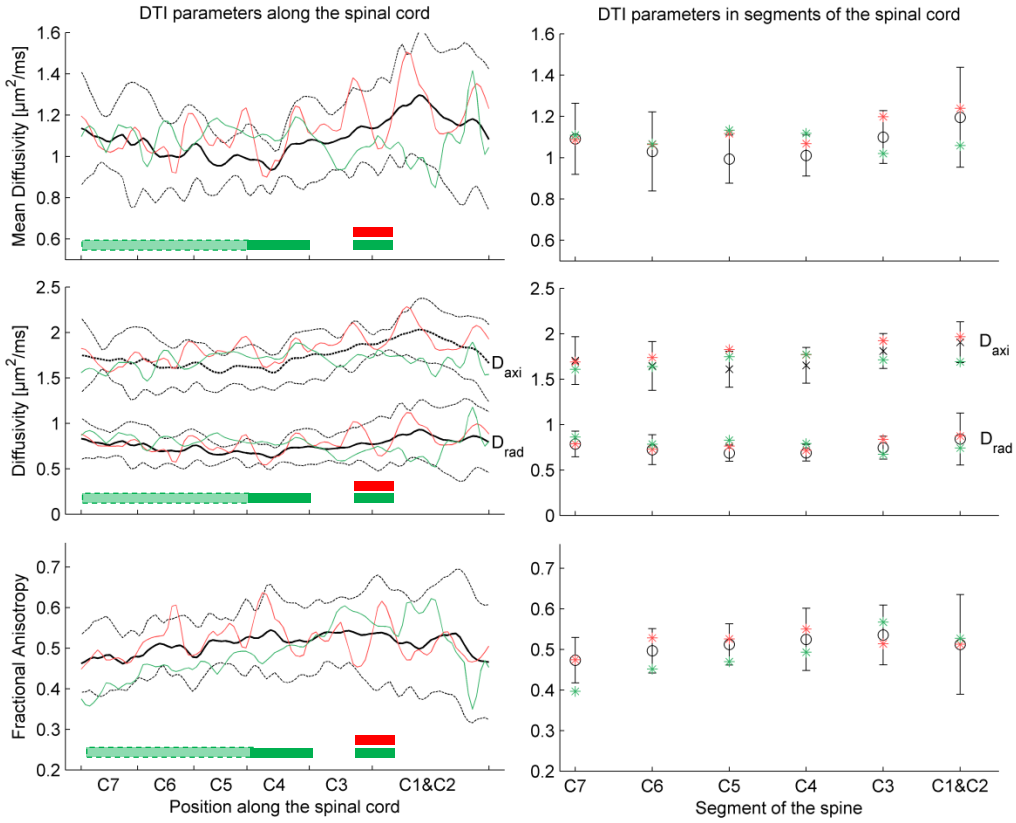

Figure 19 – Line plots on the left show MD (top row), D_{rad} and D_{axi} (center row) and FA (bottom row). Bold black lines are the mean parameter values from the healthy volunteers as a function of position along the spinal cord; broken lines show two standard deviations from the mean. Colored lines are the patient parameters along the cord and the rectangles signify the locations of lesions found in the high resolution T2-weighted images. The rectangle with dashed borders marks the area where many diffuse lesions were found in Patient B. On the right side the same data is condensed and presented in segments of the spine. Patient A. and B. are presented in red and green respectively. Note that the resulting parameter lines for the patients have a high variability, like the results seen in Figure 13, making it hard to discern between actual changes due to disease inflicted tissue as opposed to random fluctuation due to low measurement specificity.

5 Discussion

5.1 Acquisition design

The proposed acquisition design is based primarily on prior knowledge of DTI in the brain as well as DTI parameter setup in contemporary papers. The voxel size was specifically chosen to be isotropic to not introduce orientational bias in the DTI parameters [50]. The volume of the voxels combined with the 64 diffusion encoding directions and a *b*-value of 800 s/mm^2 performed a result that was consistently reproducible without serious influence due to low SNR.

Other parameters were optimized with respect to acquisition time and image distortions *i.e.* minimizing the TE and TR as well as maximizing the bandwidth. The time constraint was met even with incorporated reference imaging and high resolution T2-imaging, allowing the protocol to be appended within clinically feasible scan times.

The choice of sagittal imaging is perhaps the most influential when comparing acquisition times. The spine is an oblong structure, aligning it with the image plane allows for its entire volume to be acquired in a relatively low number of slices, dramatically lowering the acquisition time compared to a transversal slice orientation. In this method 13 sagittal slices were used equating to a FOV depth of 26 mm. This was proven to be enough in all cases although some subjects needed to be repositioned due to a RL pivoting of the head. In the case of an unusual undulation in the RL direction it was possible to expand the depth of the FOV increasing the scan time accordingly, though this was never necessary in this study. Coronal slices are possible as well, the downside is that the spine usualy undulates in the AP direction increasing the number of slices needed.

It is technically possible to align the phase encoding in the IS or RL direction although this would have an effect on the available bandwidth per pixel, aditionally there could be issues with wrapping artefacts. Chosing the AP direction for the phase-encoding is unfortunate due to the physiological movement inflicting ghosting artefacts in the AP direction, crossing the spine, but is favorable due to the smaller size of the subject in this direction.

Using acquisition tools such as dynamic field correction, field adjustment and a saturation band was imperative to image quality.

Initially the main problem with image quality was caused by eddy-currents. This was seen as a signal shift in the phase encoding direction that had varying magnitude depending on the pulsed gradient direction leading to a signal dispersion in the reconstructed parameter maps. The tensor field, in the abscense of eddy-current correction, was heavily distorted and unusable for qualitative inspection as well as segmentation. This was quite effectively remedied by engaging the DFC. This correction is a built-in optional imaging tool based on a non-affine field distortion correction, registering the diffusion weighted images to the undistorted b0 image [42]. Note that the b0 images are only concidered to be undistorted with respect to the eddy-currents, due to the absence of diffusion encoding gradients.

A possible improvement to the DTI sequence would be to incorporate the reveresed k-space read-out technique first suggested by Chang *et al.* [51]. By acquiering the diffusion weighted images twice for every diffusion encoding direction, reading the k-space for each image, in a pair, in opposite directions. This allows for a corrected image to be calculated without the need for additional reference series. It has already been demonstrated, by Voss *et al.*, that this technique improves the results of a DTI of the spine generating better WM tractography [39].

5.2 Data processing

The reconstruction parameter setup, like the imaging design, was based on prior experience in DTI of the brain as well as contemporary literature.

The most important methodological decision, concerning parameter evaluation, was to use the DTT as a segmentation method for the spine. The reasons for this were twofold. As stated by Van Hecke *et al.* [6] the use of ROI definition in the spine for DTI parameter extraction is both extremely laborious, highly dependent on the user and has a low reproducibility when compared to tractography based segmentation. The second reason was the opportunity to calculate DTI parameters as a function of anatomical location. In committing to this it was within reach to automate large portions of the evaluation. Pre-defined parameters tuned to the spine allowed for all sets of data to be processed without any significant effort. The most laborious instance of processing was the delineation of landmarks to facilitate the co-registration of parameter vectors in QuTE. Technically the delineation of two landmarks would suffice to roughly co-register all the spinal cords by scaling them linearly across the length between the first and seventh cervical vertebrae. Instead seven landmarks were defined in order to be able to divide the spinal cord in to segments corresponding to each vertebra, compounding the first and second due to their interleaved geometry.

The second most important decision was to use track length thresholding as the primary filter for track selection. It is quite intuitive that the spine should be the only structure in the suggested FOV that contains long tracks. This selection method showed great promise but proved to be significantly impaired by the local field inhomogeneity, ushering in the creation of the GDC. The GDC is discussed further in the validation section.

Beyond the well known limitations of the DT model the method suggested in this work suffers from a principal flaw in that it does not segment the WM specifically, but rather combines WM and GM into one body. This means that the tractographies produces are segmenting the entire spinal structure and not only the WM as would be expected when seeding in high FA voxels and eliminating short tracks. This is explained by two simple facts. Firstly the spine is a small and heterogenous structure compared to the spatial resolution of the DTI and so the signal from WM and GM will be inadvertently mixed creating a large volume of high FA voxels. Secondly the FA of GM has been shown to be much greater that that expected in isotropic tissue [4, 22], thus it gives rise to tracts parallel to the WM even at higher resolutions.

This has implications on how the DTI parameters can be compared when compounded into position or segment specific values since they will allways include both tissue types. The separation of spine tissue sub-types has been reported by several groups [4, 12, 22] but it is important to note that none of these report acquisition based on isotropic voxels, the entire cervical spine *and* clinically feasible scan times as part of the same protocol.

A possible sollution to this problem is to increase the FA threshold when definind seeding voxels. This could eliminate GM from the tracking. The main problem with this sollution is that it would also risk eliminating the voxels that were inflicted with a pathology that lowers the FA, such as MS. Thus it is an aceptable compromise to include the GM to maintain the ability to include pathological tissue in the segmentation.

As mentioned in 5.1, the customization of the DTI read-out technique could be used to correct for the field inhomogeneity issues described in this work. This would circumvent the need to employ the GDC and could possibly generate better tractographies. Further improvements can be expected when employing a competent motion correction, which was not available during this project. In the *in vivo* study there were examples indicating image misalignment due to movement that could have been the source of degraded tractograpy. Improving the tractography quality is not only for the sake of the visual evaluation. It could also be benefitial for more effective segmentation methods. An alternative to the length thresholding method could, for example, be to define two ROIs at the inferior and superior part of the spine. Using "and" semantics this would leave only tracks penetrating both ROIs. This is similar to the track length thresholding but could posibly be easier to implement.

5.3 System validation

In a scanner with a theoretically ideal gradient system the MD plot in Figure 10 would be constant, showing that water at equilibrium has the same MD throughout the volume. In this case the ROI method shows that it is not constant but rather a concave function with a peak MD value at the center of the FOV.

Evaluating the results of the tractography based evaluation is more complicated in nature due to the fact that there is no reference that can be said to represent the *true* DTI values of the primary cord. This means that all visible features in Figure 11 could practically be caused by constructional characteristics of the cord rather than gradient discrepancies. Nevertheless, in the absence of a reference, it is interesting to speculate at the possible correlation between the ROI method and tractography method results.

The overall concave shape of the tractography MD curve is very similar to that measured in the free water volume suggesting that the shape is not caused by constructional circumstances. A feature that is more likely to arise due to mechanical circumstances is the abrupt decrease in MD at the center of the cord. Combined with the high FA, at the same location, it is plausible that this is caused by an unintentionally hard compaction of the fibers at the center of the cord.

The fact that the FA in free water is elevated at the peripheral parts of the cord suggests that the measured FA in a perfectly homogenous fiber bundle would also increase at the edges. This effect can be partially attributed to the varying SNR, but could also indicate that the gradient influence on calculated diffusivity is not directionally invariant imposing a bias on anisotropy as well as diffusivity. Acquiring reference DTI parameters in the phantom would allow using it to quantify the effect of gradient imperfections on both all DTI parameters.

The fact that the measured MD at the center and peripheral parts of the FOV differ more than 10 % is strongly indicative of a gradient performance issue. Although discrepancies such as this are common this spatial dependency can quite possibly bias diffusion measurements performed *in vivo*. This discrepancy warrants further investigations with special consideration to the effect on DTI parameter quantification *in vivo* and possible improvements that can minimize the inflicted error.

The SNR in the spine and phantom was expected to be lower in the inferior parts of the FOV because the signal would have its origin farther away from the receiver coils as is demonstrated in Figure 12. The *in vivo* SNR does not exhibits a strict decrease of SNR going from superior to inferior regions. Instead the SNR is the lowest in the region of the third and fourth cervical vertebrae. A possible explanation for this is that the DTI model fit in this region is impaired by distortions caused by the physiological movement in the esophagus although no such indications are present in the DTI images. Further no direct conclusions can be drawn from comparing the phantom SNR to the *in vivo* SNR due to the fact that the experiment is affected by RF energy deposition, water content in the respective cords and influence from physiological movement.

Further investigations are warranted to quantify the correlation of DTI parameter bias and the estimated SNR suggested in this method. Having this information could be used as post-hoc image quality control as well basis for imaging sequence optimization.

The primary goal of the reproducibility study was to gain a base knowledge of the minimum variability that was practically achievable in a standard acquisition. This is the reason for the measurement to be performed in five consecutive acquisitions without having the subject exit and reenter the scanner. Observing the fluctuations on the left side of Figure 13 it can be seen that the variation is in the order of 10 to 20 %. It is therefore unlikely that this method could be used to detect MS lesions on an individual basis. Further investigations should be performed to find the origin of these fluctuations, possibly eliminating them by employing techniques such as gating.

The analysis of the correction vector for the five repeated DTI series shows that the segment between the first and second cervical vertebrae was corrected in different ways in each acquisition, varying as much as 5 mm. This is not believed to be a flaw in the algorithm but rather a statement to the varying inhomogeneity of the magnetic field. It is plausible that the influence from the involuntary movement of the pharynx have perturbed the local field differently in the five acquisitions thus giving rise to five different corrections.

The correction method suggested in this work was based on a simple image matching algorithm performing a signal shift in one dimension based on the theoretical considerations explained in 2.5, specifically in Eq. 5. Assuming that the geometrical distortion is, in fact, an effect of local field inhomogeneity in the main magnetic field, it is justifiable to shift signal along the phase encoding direction. Further it is assumed that a TSE sequence, with matching contrast, is a good reference for this type of image matching [46].

With very little addition to the computational time the GDC was able to produce an improved tractography in all cases that were evaluated. When quantifying the quality before and after correction the total number of remaining tracks after length thresholding was used. It is important to note that the number of tracks in a tractography is not necessarily indicative of higher quality since fragmentation, which can be an effect of a poorly aligned tensor field, produces a higher number of tracts. When using a track length threshold the focus is not so much on track fragmentation but the presence of tracks that have successfully traversed a long distance in the cord, indicating a well aligned tensor field, which is associable to good quality. The purpose of creating a quality measure is not to validate tractography in general but rather to create a reference of quality with respect to this particular method, keeping in mind that it is dependent on the subsequent spatial analysis performed in QuTE.

The evaluation of track coherence relative to the reference images is yet another statement to the advantage of the correction. The fact that the tract geometry that best fits the reference also generates higher quality tractography is evidence to support that the initial assumption, as to the reason for distortion, is correct.

As stated in Figure 17 there are signs of sub-optimal correction. It is quite possible that the correction algorithm can be further optimized and allow for more strict length thresholding or the two ROI selections mentioned above.

Finally it must be noted that the implications of implementing the GDC are not entirely known. A possible confounder is the pixel shift performed during correction. It has a smoothing and diluting effect due to the fact that voxel signal intensity is translated in fractions of pixels. This is further complicated by the fact that the translation is only ever present in the AP direction, making it spatially variant even within the same axial slice. The main effect expected from this is the loss of contrast in the AP direction, possibly increasing the PVE.

5.4 In vivo pilot study

The *in vivo* pilot study was successfully performed as proof of concept that it is possible to facilitate the necessary acquisition, data processing and evaluation of DTI data. The method draws from the reported experience of several papers concerning DTI in the spine [4, 6, 11, 15, 16, 18-20, 22, 27, 39] but is differentiated by its clinical premise and comprehensive scope, solving problems even beyond the acquisition of data.

The comparison of two patients to a normal material of eleven volunteers is obviously lacking in power to show any statistically significant difference in DTI

parameters between the groups but the ability to look at individual patient results as a function of position along the cervical spine invites the use of DTI as a diagnostic method on an individual basis. This notion is attractive although presently unavailable due to the large inter and intra patient variability as well as an intrinsic variability in the system, as described in the reproducibility results.

The presentation of parameters as a function of position is only ever advantageous if considering comparison of individual data to a normal material or if the pathology in question has a proclivity to involve tissue at a certain location. In the present case the possibility to compare individual data to a normal material would be valuable only if the intra and inter subject variability was low enough to allow detection of local tissue damage. This means that the suggested method is a strong candidate for larger group comparisons but must be improved to provide useful information on an individual basis.

As detailed above the GDC improved the tractography in all subjects although one set of data had to be excluded from the evaluation due to incomplete tracking in the region of the first cervical vertebrae. Fortunately the circumstances allowed for repeated measurements, showing a reproducible fault in the tracking. The shape of the track bundle coming from the inferior direction expressed a "Y-shape", failing to connect the cervical spine to the medulla oblongata. The spine of the volunteer was confirmed to be healthy in the high resolution images. The reason for this tensor field discrepancy is still unknown.

6 Conclusion

This project aimed to answer the question if it was possible to implement a clinically adapted DTI protocol of the cervical spine. In answering this question, methods for acquisition, processing, correction and evaluation were proposed. These methods were evaluated by performing validation tests as well as a pilot *in vivo* study.

Validation showed that the inter acquisition variability for one volunteer was in the order of 10 to 20 % at any point along the spine, implying that this method lacks the precision needed to perform individual diagnostics on MS patients. The validation also showed that the resulting DTI parameters could be inaccurately quantified due to system gradient performance, although the exact effect of this on *in vivo* studies is not known.

The *in vivo* pilot study proved the suggested methods to be viable in a clinical setting; adding only 5 minutes to the standard scan time and allowing for quick and highly automated evaluation of data which could be used for large group comparisons.

The study also advanced our understanding of the limitations and possibilities of the MRI system with respect to DTI as well as related diffusion based imaging. With this knowledge it is possible to further improve on the current method as well as develop methods for future trials.

Acknowledgements

My most sincere and grateful thanks go out to my supervisors. Without them this project would not have been as inspired and ambitious and I consider myself lucky to have received their indispensable help and support.

I would also like to thank all of the volunteers and medical staff for lending their time to make all of the experiments possible.

Finally, I thank my family for all the much needed support!

Bibliography

1. Beaulieu, C., *The basis of anisotropic water diffusion in the nervous system - A technical review*. NMR in Biomedicine, 2002. **15**(7-8): p. 435-455.
2. Mori, S. and P.C.M. Van Zijl, *Fiber tracking: Principles and strategies – A technical review*. NMR in Biomedicine, 2002. **15**(7-8): p. 468-480.
3. Jones, D.K. and M. Cercignani, *Twenty-five pitfalls in the analysis of diffusion MRI data*. NMR in Biomedicine, 2010. **23**(7): p. 803-820.
4. Onu, M., *et al.*, *Human cervical spinal cord funiculi: Investigation with magnetic resonance diffusion tensor imaging*. Journal of Magnetic Resonance Imaging, 2010. **31**(4): p. 829-837.
5. Moseley, M.E., *et al.*, *Early detection of regional cerebral ischemia in cats: Comparison of diffusion- and T2-weighted MRI and spectroscopy*. Magnetic Resonance in Medicine, 1990. **14**(2): p. 330-346.
6. Van Hecke, W., *et al.*, *A tracking-based diffusion tensor imaging segmentation method for the detection of diffusion-related changes of the cervical spinal cord with aging*. Journal of Magnetic Resonance Imaging, 2008. **27**(5): p. 978-991.
7. Vargas, M., *et al.*, *Clinical applications of diffusion tensor tractography of the spinal cord*. Neuroradiology, 2008. **50**(1): p. 25-29.
8. Klein, J.C., T.E.J. Behrens, and H. Johansen-Berg, *Connectivity fingerprinting of gray matter*, in *Diffusion MRI*, T.E.J. Behrens and H. Johansen-Berg, Editors. 2009, Elsevier Inc. p. 377-402.
9. Jones, D.K., *et al.*, *Non-invasive assessment of axonal fiber connectivity in the human brain via diffusion tensor MRI*. Magnetic Resonance in Medicine, 1999. **42**(1): p. 37-41.
10. Lebel, C., *et al.*, *Microstructural maturation of the human brain from childhood to adulthood*. NeuroImage, 2008. **40**(3): p. 1044-1055.
11. Rajasekaran, S., *et al.*, *Diffusion tensor tractography demonstration of partially injured spinal cord tracts in a patient with posttraumatic brown sequard syndrome*. Journal of Magnetic Resonance Imaging, 2010. **32**(4): p. 978-981.
12. Smith, S.A., *et al.*, *Reproducibility of tract-specific magnetization transfer and diffusion tensor imaging in the cervical spinal cord at 3 tesla*. NMR in Biomedicine, 2010. **23**(2): p. 207-217.
13. Basser, P.J., J. Mattiello, and D. LeBihan, *MR diffusion tensor spectroscopy and imaging*. Biophysical Journal, 1994. **66**(1): p. 259-267.
14. Biton, I.E., I.D. Duncan, and Y. Cohen, *q-space diffusion of myelin-deficient spinal cords*. Magnetic Resonance in Medicine, 2007. **58**(5): p. 993-1000.
15. Clark, C.A., G.J. Barker, and P.S. Tofts, *Magnetic resonance diffusion imaging of the human cervical spinal cord in vivo*. Magnetic Resonance in Medicine, 1999. **41**(6): p. 1269-1273.
16. Mamata, H., F.A. Jolesz, and S.E. Maier, *Apparent diffusion coefficient and fractional anisotropy in spinal cord: Age and cervical spondylosis–related changes*. Journal of Magnetic Resonance Imaging, 2005. **22**(1): p. 38-43.
17. Clark, C.A. and D.J. Werring, *Diffusion tensor imaging in spinal cord: Methods and applications - A review*. NMR in Biomedicine, 2002. **15**(7-8): p. 578-586.
18. Van Hecke, W., *et al.*, *A diffusion tensor imaging group study of the spinal cord in multiple sclerosis patients with and without T2 spinal cord lesions*. Journal of Magnetic Resonance Imaging, 2009. **30**(1): p. 25-34.
19. Benedetti, B., *et al.*, *A diffusion tensor MRI study of cervical cord damage in benign and secondary progressive multiple sclerosis patients*. Journal of neurology, neurosurgery and psychiatry, 2010. **81**(1): p. 26-30.
20. Filippi, C.G., *et al.*, *Magnetic resonance diffusion tensor imaging and tractography of the lower spinal cord: Application to diastematomyelia and tethered cord*. European Radiology, 2010. **20**(9): p. 2194-2199.
21. Balbi, V., *et al.*, *Tractography of lumbar nerve roots: Initial results*. European Radiology, 2011. **21**(6): p. 1153-1159.

22. Ellingson, B.M., *et al.*, *Diffusion tensor MR imaging of the neurologically intact human spinal cord.* American Journal of Neuroradiology, 2008. **29**(7): p. 1279-1284.
23. Inglese, M. and M. Bester, *Diffusion imaging in multiple sclerosis: Research and clinical implications.* NMR in Biomedicine, 2010. **23**(7): p. 865-872.
24. Rovaris, M., *et al.*, *Diffusion MRI in multiple sclerosis.* Neurology, 2005. **65**(10): p. 1526-1532.
25. Filippi, M. and A. Rocca Maria, *MR Imaging of Multiple Sclerosis.* Radiology, 2011. **259**(3): p. 659-681.
26. Rovaris, M. and M. Filippi, *The role of magnetic resonance in the assessment of multiple sclerosis.* Journal of the Neurological Sciences, 2000. **172**(-Supplement_1): p. S3-S12.
27. Valsasina, P., *et al.*, *Mean diffusivity and fractional anisotropy histogram analysis of the cervical cord in MS patients.* NeuroImage, 2005. **26**(3): p. 822-828.
28. Schwartz, E.D. and A.E. Flanders, *Spinal trauma: Imaging, diagnostics and management*. 2007, Philadelphia: Lippincott Williams & Wilkins.
29. Landman, B.A., *et al.*, *Effects of diffusion weighting schemes on the reproducibility of DTI-derived fractional anisotropy, mean diffusivity, and principal eigenvector measurements at 1.5T.* NeuroImage, 2007. **36**(4): p. 1123-1138.
30. Åslund, I., *Measuring material properties through gradient based NMR: Diffusion and imaging*, in *Division of Physical Chemistry*. 2010, Lund University: Lund.
31. Price, W.S., *Pulsed-field gradient nuclear magnetic resonance as a tool for studying translational diffusion: Part 1. Basic theory.* Concepts in Magnetic Resonance, 1997. **9**(5): p. 299-336.
32. Le Bihan, D. and P.J. Basser, *Molecular Diffusion and Nuclear Magnetic Resonance*, in *Diffusion and perfusion magnetic resonance imaging*, D. Le Bihan, Editor. 1995, Raven Press, Ltd.: New York. p. 5-17.
33. Le Bihan, D., *et al.*, *MR imaging of intravoxel incoherent motions: Application to diffusion and perfusion in neurologic disorders.* Radiology, 1986(161): p. 401-407.
34. Stejskal, E.O. and J.E. Tanner, *Spin diffusion measurements: Spin echoes in the presence of a time-dependent field gradient.* The Journal of Chemical Physics, 1964. **42**(1): p. 288-292.
35. Le Bihan, D. and P.J. Basser, *Molecular diffusion and nuclear magnetic resonance*, in *Diffusion and perfusion magnetic resonance imaging*, D. Le Bihan, Editor. 1995, Raven Press, Ltd.: New York.
36. Alexander, D.C., *Modelling, fitting and sampling in diffusion MRI*, in *Visualization and processing of tensor fields*, D. Laidlaw and J. Weickert, Editors. 2009, Springer Berlin Heidelberg. p. 3-20.
37. Lätt, J., *et al.*, *Effects of restricted diffusion in a biological phantom: A q-space diffusion MRI study of asparagus stems at a 3T clinical scanner.* Magnetic Resonance Materials in Physics, Biology and Medicine, 2007. **20**(4): p. 213-222.
38. Behrens, T.E.J. and S. Jbabdi, *MR diffusion tractography*, in *Diffusion MRI*, H. Johansen-Berg and T.E.J. Behrens, Editors. 2009, Elsevier Inc. p. 333-352.
39. Voss, H.U., *et al.*, *Fiber tracking in the cervical spine and inferior brain regions with reversed gradient diffusion tensor imaging.* Magnetic Resonance Imaging, 2006. **24**(3): p. 231-239.
40. Pipe, J., *Pulse sequense for diffusion-weighted MRI*, in *Diffusion MRI*, H. Johansen-Berg and T.E.J. Behrens, Editors. 2009, Elsevier Inc. p. 11-36.
41. Basser, P.J. and E. Özarslan, *Introduction to Diffusion MR*, in *Diffusion MRI*, H.B. Johansen-Berg, T.E.J., Editor. 2009, Elsevier Inc.: London.
42. Wagegg, D., *Siemens internal document: News for DWI*. 2011, Siemens.
43. Fillard, P., *et al.*, *Quantitative evaluation of 10 tractography algorithms on a realistic diffusion MR phantom.* NeuroImage, 2011. **56**(1): p. 220-234.
44. Wang, R. and V.J. Wedeen, *Diffusion Toolkit (Version 0.6.1)*. 2010, Martinos Center for Biomedical Imaging.
45. Wang, R. and V.J. Wedeen, *TrackVis (Version 0.5.1 Public)*. 2010.

46. Wu, M., *et al. Comparison of EPI distortion correction methods in diffusion tensor MRI using a novel framework*. in *Medical Image Computing and Computer-Assisted Intervention – MICCAI 2008*. 2008. New York, NY, USA: Springer.
47. Mårtensson, J., *Improved analysis of MRI tractography data: Group comparisons of parameters along fibre tracks*, in *Department of Medical Radiation Physics*. 2010, Lund University: Lund.
48. Mårtensson, J., *et al. Spatial analysis of diffusion tensor tractography depicts local white matter changes*. in *Proc. Intl. Soc. Mag. Reson. Med. 2010; 4876*. 2010.
49. Santarelli, X., *et al.*, *Dependence of the fractional anisotropy in cervical spine from the number of diffusion gradients, repeated acquisition and voxel size.* Magn Reson Imag, 2009. **28**(1): p. 70-76.
50. Oouchi, H., *et al.*, *Diffusion Anisotropy Measurement of Brain White Matter Is Affected by Voxel Size: Underestimation Occurs in Areas with Crossing Fibers.* 2007. **28**(6): p. 1102-1106.
51. Chang, H. and J.M. Fitzpatrick, *A technique for accurate magnetic resonance imaging in the presence of field inhomogeneities.* Medical Imaging, 1992. **11**(3): p. 319-329.